**Title**
RANGE-ENERGY RELATION FORAu IONS, E < 152 MeV/amu



**Author**
Heckman, H.H.

**Publication Date**
1985

# Lawrence Berkeley Laboratory
UNIVERSITY OF CALIFORNIA



Invited talk presented at the Second
International Workshop on Atomic Physics
for Ion Fusion, Chilton, Oxon, United Kingdom,
September 11-14, 1984

RANGE-ENERGY RELATION FOR Au IONS, $E \leq 152$ MeV/amu

H.H. Heckman, H.R. Bowman, Y.J. Karant,
J.O. Rasmussen, A.I. Warwick and Z.Z. Xu

January 1985

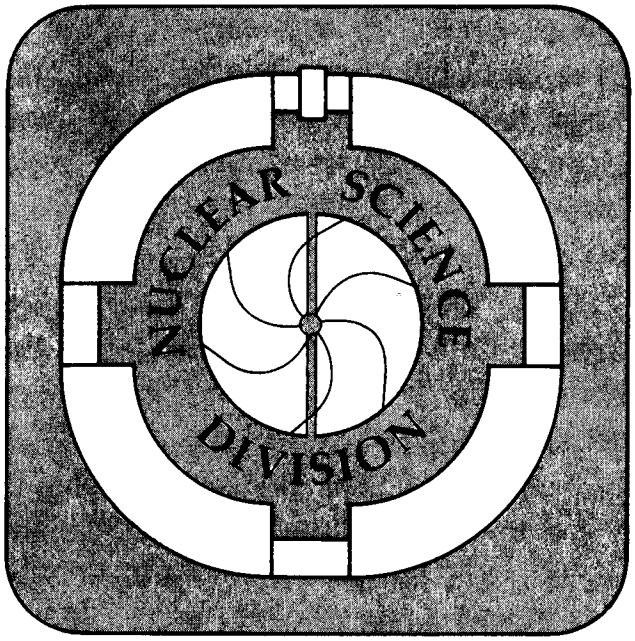






Prepared for the U.S. Department of Energy under Contract DE-AC03-76SF00098

## DISCLAIMER

LBL-19031

# Range-Energy Relation for Au Ions, E $\leq$ 152 MeV/amu

H.H. Heckman, H.R. Bowman,[‡] Y.J. Karant, J.O. Rasmussen,
A.I. Warwick[†] and Z.Z. Xu[*]

Nuclear Science Division
Lawrence Berkeley Laboratory
University of California
Berkeley, California 94720

Invited talk for the Second International Workshop on Atomic Physics for Ion Fusion, Rutherford Appleton Laboratory, Chilton, Oxon, United Kingdom, September 11-14, 1984.

This work was supported by the Office of Energy Research, jointly by the Division of Nuclear Physics of the Office of High Energy and Nuclear Physics and by the Office of Basic Energy Sciences of the U.S. Department of Energy under Contract DE-AC03-76SF00098.

[‡]Earth Sciences Division

[†]Accelerator & Fusion Research Division

[*]on leave from Fudan University, Shanghai, China

# Range-Energy Relation for Au Ions, E ≤ 152 MeV/amu

H.H. Heckman, H.R. Bowman,‡ Y.J. Karant, J.O. Rasmussen,
A.I. Warwick† and Z.Z. Xu*

Nuclear Science Division
Lawrence Berkeley Laboratory
University of California
Berkeley, California 94720

## Abstract

The first results of a Bevalac experiment on the range-energy (R-E) relation of Au beam nuclei, E ≤ 152 MeV/amu, in CH and Au absorbers are reported. The measured ranges are found to agree, within ≈±2%, on the average, with those predicted by a R-E relation based on the phenomenology introduced by Barkas and Berger. The energy-loss rate and effective charge versus energy are also presented.

The capability of the Bevalac for producing high-rigidity, low-charge-state beams applicable to heavy ion inertial fusion, and their planned use for range-energy experiments, is described.

This work was supported by the Office of Energy Research, jointly by the Division of Nuclear Physics of the Office of High Energy and Nuclear Physics and by the Office of Basic Energy Sciences of the U.S. Department of Energy under Contract DE-AC03-76SF00098.

‡Earth Sciences Division
†Accelerator & Fusion Research Division
*on leave from Fudan University, Shanghai, China

Introduction:

Of major importance to the problem of ion-target coupling for Heavy Ion Fusion (HIF) is the range-energy relation for heavy ions, e.g. Au, in hot (and cold) matter.[1] A unique feature of heavy ion beams for HIF, $E \leq 150$ MeV/amu, is the very low charge state at which they will be accelerated, e.g., at $Z_{accel} = +1$ or $+2$. Such beams, upon penetrating the target, will have ionic charge states far from equilibrium values characteristic of their velocity $\beta$ and the target material. As a consequence, both the rate of energy loss, $dE/dx$, and the effective charge, $Z^*$, of the incident heavy ions in matter will be low initially, but will increase as they approach their equilibrium values as electron-stripping takes place. The effects of the diminished values of $dE/dx$ and $Z^*$ of the incident heavy ions will thus tend to increase the range of the ions in the stopping material.

We have begun experiments at the Bevalac to obtain range-energy data pertinent to HIF; specifically, the range-energy relation for Au ions, $E \lesssim 150$ MeV/amu, accelerated and incident on targets at charge states $11 \leq Z_{accel} \leq 61$. The experiments will focus on the dependence of $dE/dx$, hence the effective charge $Z^*$ of Au ions in matter as a function of the initial charge state of the beam $Z_{accel}$, beam energy, and residual range in the energy interval $10 \lesssim E \lesssim 150$ MeV/amu. The target materials are CH and Au, representative of HIF targets that are designed to utilize the different energy-absorbing properties of low- and high-Z materials.

Low-Charge-State Beams at the Bevalac:

A crucial aspect of these experiments is the availability of low-charge-state, high rigidity beams of heavy nuclei at the Bevalac. The

limitations of the maximum beam rigidities that can be transmitted by the transfer line from the Hilac ($p/Z_{accel}$ = 0.46 GeV/c) and accelerated in the Bevatron ($p/Z_{accel}$ = 5.75 GeV/c), establish the maximum energies of injection and extraction for given values of $Z_{accel}$. Table I gives several representative values of these energies for Au ions injected and accelerated at $Z_{accel}$ to $p_{max}$ = 5.75 $Z_{accel}$ GeV/c. The values of E(max) for $Z_{accel}$ = 61, 35 and 11 are specifically listed because the energies for which these charge states are available from the Hilac are equal to, or less than, those set by the rigidity limits of the transfer line.

An additional operational requirement to be met at the Bevatron is that the dynamic range of acceleration frequencies necessary to accelerate an ion beam from injection to extraction energies be within the interval $210 \leq \nu \leq 2500$ kHZ. This restriction allows the ions to be accelerated on a single harmonic, thereby avoiding the need for the switching of harmonics during acceleration. Under these conditions the maximum velocities that can be extracted when accelerating under the $n^{\underline{th}}$ harmonic is $\beta = 1/n$. Thus, the acceleration of $Au^{+11}$ to 50 MeV/amu must be carried out using the $3^{\underline{th}}$ harmonic

Table I: Beam parameters for Au ions accelerated at charge $Z_{accel}$. At B(max) = 12.575 kG, $p_{max}$ = 5.75 $Z_{accel}$ GeV/c.

| $Z_{accel}$ | $E_{injection}$(max) (MeV/amu) | $E_{extraction}$(max) (MeV/amu) | $\beta$ | Harmonic |
|---|---|---|---|---|
| 61 | 8.5 | 1077 | 0.886 | $1^{\underline{st}}$ |
| 35 | 3.63 | 451 | 0.739 | $1^{\underline{st}}$ |
| 11 | 0.358 | 53.8 | 0.326 | $3^{\underline{rd}}$ |

(i.e. three separate bunches of ions are accelerated simultaneously), with extraction taking place at nearly the maximum rigidity of the Bevatron.†

Figure 1 presents the maximum beam energy, expressed in E(max)/amu, as a function of $Z_{accel}$. The (top) curve labeled $Z^*_{equil}$ is the calculated effective equilibrium charge of Au ions in a CH target. The curve giving the excess number of electrons, $Z^*_{equil} - Z_{accel}$, shows that Au beams can have up to 63 electrons in excess of the number expected under equilibrium conditions in the energy interval of the experiment, $20 \leq E \leq 152$ MeV/amu.

The essence of this experiment is illustrated by the dashed curve in Fig. 1, which indicates schematically a possible trajectory of the transition of Z* from $Z_{accel} = 19$ to $Z^*_{equil}$ for $^{197}Au$ incident on CH at E = 152 MeV/amu as it loses energy by ionization. Note that electron configurations through the N, M and L shells occur when beam energies are below 150 MeV/amu, hence will simulate well the stopping phenomena to be associated with HIF beams. Because the valence electrons will be lost rapidly from low-charge state ions as they penetrate the target material, their initial presence will probably have little effect on the range-energy (R-E) relation. More important to the R-E relation, we expect, will be the stripping of the inner-shell electrons, a subject that can be addressed by experiments at the Bevalac.

Experimental Configuration and Techniques:

A schematic drawing of the experimental arrangement in place at the Bevatron. Beam-40 has a magnetic spectrometer that provides for TOF

---

†Post workshop development: In November, 1984, the Bevalac accelerated ions on the 3rd harmonic for the first time. $Au^{+11}$ ions were subsequently accelerated and extracted at 50 MeV/amu. Maximum beam intensities were typically $10^4$ ions per pulse.

measurements of beam particles over a distance of 21 m. The spectrometer can be used with a position-sensitive wire chamber to measure the charge spectrum $Z_i(\beta)$ of the primary and secondary (energy-degraded) beams by magnetic analysis.

The range-energy data are obtained by measurements of the following quantities:

i) Beam velocities, hence energies, by time of flight (TOF). With time resolution $\delta t \sim 0.2 \times 10^{-9}$s over a 21 m flight path, $\Delta E/E < 1\%$.

ii) dE/dx by measurements of $\Delta E$ (TOF) vs foil thickness $\Delta x$.

iii) Integral ranges by use of circular, wedge shaped absorbers with visual track detectors.

iv) Charge spectra of beam ions $Z_i(\beta)$ by use of magnetic spectrometer.

To minimize the effects of energy-loss and perturbation of the charge state of the incident beam introduced by the start-counter $S_1$, Fig. 2, we have used scintillators of thickness 0.2 and 0.5 mg/cm$^2$ viewed by two diametrically opposed 8575 photomultipliers. Stop-counter $S_2$ was of the same design, having a 0.5 mg/cm$^2$ scintillator. With this configuration, we obtained a time resolution of $\approx 0.2 \times 10^{-9}$ sec (FWHM), which, for a flight path of 21 m, yields kinetic energies whose accuracies are, presently, limited primarily by the systematic uncertainty in the absolute calibration of the TOF estimated to be $\Delta t$ (systematic) $\approx \pm 0.3 \times 10^{-9}$. This uncertainty leads to a systematic error $\Delta E \approx \pm 0.2$ MeV/amu at 50 MeV/amu.

The ranges of the Au ions at energies $E \gtrsim 20$ MeV/amu are measured directly by the use of circular, wedge-shaped absorbers made of CH and Au,

backed by 10 μm-thick nuclear emulsion detectors to record the location of the end-points of the ranges of the incident ions in the absorbers. Fig. 3a shows the cross-section of the "washer-shaped" CH wedge, with a glass-backed nuclear emulsion detector placed in contact with the plane (back)-surface of the wedge. Fig. 3b is a photograph of the emulsion detector that was in contact with the CH wedge and exposed at normal incidence to the primary $Au^{+61}$ beam at E = 152 MeV/amu. For wedge-thickness less than the range of the Au nuclei in CH at this energy the ions will exit the wedge, penetrate the emulsion detector and will be observed as continuous ionization tracks that enter and exist normal to the emulsion plate. The circular pattern of transmitted ions terminates along a circumference whose radius is geometrically related to the range of the incident ion in the absorber. The radius r is determined i) by measuring the xy coordinates of the Au ions that are observed to stop in the 10 μm-thick emulsion plate, and ii) by subjecting these data to a least-squares fit to obtain the mean radius r and the standard deviation of the radial distribution.

Fig. 3c presents the radial distribution of stopping Au nuclei deduced from the emulsion plate, Fig. 3b. The mean range R of the incident Au ions is given by:

$$R = \rho \tan\alpha \, (r - r_0) - \delta \ (gm/cm^2) \quad , \tag{1}$$

where $\rho$ = density of absorber material,

$\alpha$ = angle of wedge,

$r_0$ = radius of wedge at (i.e., extrapolated to) zero thickness,

and $\delta$ = range equivalent ($gm/cm^2$) of the 5 μm half-thickness of the emulsion detector.

For the CH wedge, R is given specifically by

$$R = 0.4889\ (r - 0.6312) + 0.0008 \quad gm/cm^2 \qquad (2)$$

and for the Au wedge,

$$R = 1.2815\ (r - 0.6320) + 0.0037 \quad gm/cm^2 \quad . \qquad (3)$$

The mean of the radial distribution of stopping Au ions shown in Fig. 3c is $r = 1.8377 \pm 0.0037$ (rms) cm, equivalent to a range straggle of ±0.31%. The corresponding mean range of 152.0 MeV/amu-Au ions in CH (Eq. 2) is, in this particular example, $0.5907 \pm 0.0001_3$ gm/cm$^2$.

Results:

Fig. 4 presents our first results on the range-energy relation for Au ions in CH and Au. These measurements were made using the $Au^{+61}$ beam, extracted at 152 MeV/amu. The residual ranges R indicated were obtained i) from direct measurements using the wedge absorbers only, as described above, and ii) from the differences $R_i = R_o - S_i$, where $R_o$ is the measured range of the Au ion at (primary) beam energy, as obtained in i), and $S_i$ is the thickness of the target (absorber) foil used to degrade the energy of the incident primary beam to $E_i$. The values of energy $E_i$ were obtained from the measurements of the TOF, hence, velocity β, of the Au ions after they traversed target foils of thickness $S_i$. The kinetic energies are given in units MeV/amu, defined by

$$E = 931.5016\ [(1 - \beta^2)^{-1/2} - 1] \quad MeV/amu \quad .$$

The R-E data can be fitted satisfactorily by least squares to a quadratic equation of form

$$\ell n\ R = a + b\ \ell n\ E + c\ (\ell n\ E)^2 \quad gm\ cm^{-2} \tag{4}$$

in the energy interval $20 \lesssim E \lesssim 150$ MeV/amu. These least-squares polynomials are shown in Fig. 4 as dashed lines. The standard deviations of the data points about the least-squares polynomials are $\sigma = 0.2\%$ (Au) and 0.4% (CH), dispersions that include all statistical errors attributable to the velocity and range measurements and beam instabilities. Table II gives the least-squares coefficients of the polynomials, Eq. 4, for Au ions in CH and Au.

Table II: Coefficients of the least-squares polynomial fit to the R-E data, Eq. 4, for Au ions in CH and Au; $20 \lesssim E \lesssim 150$ MeV/amu.

| Material | a | b | c |
|---|---|---|---|
| CH | -6.733 ± 0.133 | 0.8321 ± 0.0610 | 0.0803 ± 0.0069 |
| Au | -4.102 ± 0.099 | 0.2992 ± 0.0441 | 0.1127 ± .0049 |

Fig. 5 shows the energy-loss rate data, dE/dx versus E for Au ions in CH and Au. Indicated are the data for which the range differences, $\Delta X$, were obtained i) from the measured differences in the wedge ranges, $\Delta R = R_i - R_j$, and ii) from differences in the degrader-foil thicknesses, $\Delta S = S_i - S_j$, with $\Delta E = E_i - E_j$. The energy-loss rates, evaluated from the above least-squares R-E polynomial, i.e.,

$$dE/dx = AE[R(b + 2c\ \ell n\ E)]^{-1} \quad MeV/(gm\ cm^{-2}) \quad , \tag{5}$$

where A, the atomic weight of Au, is 196.9 amu, are also shown in Fig. 5 as dashed lines.

An alternative way of displaying the dE/dx data is to present it, as in Fig. 6, in terms of the effective charge Z* of the ion at velocity β, defined by the expression

$$Z^*(\beta) = \left[\frac{dE(\beta)}{dx}\ \text{ion} \Big/ \frac{dE(\beta)}{dx}\ \text{proton}\right]^{1/2} \quad . \tag{6}$$

We have evaluated the values of Z* of Au ions in CH and Au by taking $\frac{dE(\beta)}{dx}$ ion to be that given by Eq. 5, with the proton energy-loss rate, $\frac{dE(\beta)}{dx}$ proton, as derived from the range-energy relation of Barkas and Berger.[2] We find that at energies ≈150 MeV/amu the effective charges in CH and Au are approximately equal, with Z* ≈ 77.7 indicating that 1 to 2 electrons remain bound to the nucleus, on the average, at this energy. As the Au ion loses energy, Z* decreases as charge neutralization takes place. The values of Z* for Au beams in both CH and Au targets decrease with kinetic energy. The rate of neutralization of Au ions in CH (a low-Z material) is notably less than the rate in Au (a high-Z material) over the range of energies we have examined. At 20 MeV/amu, for example, the difference between the Z*'s in CH and Au targets becomes about 6.9 units of charge, e.g., 64.7 and 51.8, respectively.

Comparison of Results with a Phenomenological R-E Relation:

The R-E relation of heavy ions of mass M (in units of the proton mass) and atomic number Z at velocity β in matter can be expressed phenomenologically by

$$R(\beta) = \frac{M}{Z^2} R_p(\beta) + R_{EXT} \quad . \tag{7}$$

The range of a proton, $R_p(\beta)$, at velocity $\beta$, when scaled by $M/Z^2$, is the calculated range for a completely stripped ion, i.e., $Z^* \equiv Z$. However, because electron capture occurs when the velocity of the ion is $\lesssim \beta_K$, i.e., the velocity of the K-electron of the ion, $Z^* < Z$, in general. The rate of energy loss is diminished by electron capture for a stopping ion, thereby extending its range. The quantity $R_{EXT}$ represents this range extension. For the proton range-energy, we use the relation formulated by Barkas and Berger.[2] Basically, the Barkas-Berger R-E relation utilizes the Bethe theory, with shell and density correction terms, to fit experimental proton R-E data by adjusting the ionization potential of the stopping material. The range extension term has been deduced empirically from the heavy-ion range data ($E \leq 10$ Mev/amu) of Heckman, et al.[3] and Henke and Benton.[4] We have used the R-E code for heavy ions developed by Benton and Henke,[5] expressly written to incorporate the phenomenology of the Barkas-Berger R-E relation and the range-extension term for heavy ions.[6]

The range and dE/dx predicted from this R-E code are shown as continuous lines in Figs. 4 and 5. The values of the (adjusted) ionization potentials for CH and Ag used in the calculation were the nominal values recommended by Benton and Henke[5] for these materials, namely, $I_{adj}$ = 63.2 eV and 796.7 eV, respectively. The agreement between experiment and the predicted ranges from the R-E, Eq. 7, is good. The average differences between the calculated ranges for Au ions in CH and Au and the normal ranges are ~−2% and +2%, respectively. These differences are not outside our estimates of the cumulative systematic uncertainties in the TOF and range measurements, as well

as the estimated uncertainty (~1%) in the calculated ranges.[2] The data presented in Figs. 4 and 5 are preliminary in that, although small, systematic correction and refined TOF calibrations will be implemented as the experiment proceeds.

Summary and Outlook:

The first phase of an experiment to determine the range-energy relation for heavy nuclear beams in (cold) matter at energies $10 \leq E \leq 150$ MeV/amu has been carried out with $Au^{+61}$ ions in CH and Au targets. Current plans are to complete similar range-energy measurements for beams of $Au^{+61}$ and $Au^{+11}$ at energies $\leq$50 MeV/amu in order to investigate the dependence of the R-E relation on the charge-state of the incident beam. As illustrated in Fig. 6, Au ions, after entering a CH target at $Z_{accel} = +61$ at 152 MeV/amu, exhibit an effective, equilibrated, charge of $Z^* \approx 72$ at 50 MeV/amu. It is therefore possible to carry out range measurements for $Au^{+61}$ and $Au^{+11}$ beam ions, $E \leq$ 50 MeV/amu, which have, initially, 11 and 61 electrons, respectively, in excess of the effective number they possess at equilibrium in this material at this energy.

Following the completion of these range measurements, we shall undertake magnetic-spectrometer measurements of the charge-state distributions $Z_i(\beta)$ of the ions after they leave the target. Our intent here is to relate the "external" charge distribution $Z_i(\beta)$ with the effective "internal" charge $Z^*(\beta)$ for Au ions in a variety of target materials.

Acknowledgments:

We want to give recognition to Steven Klingler (LBL), James Bryan (LLNL) and Richard Clouser (LLNL) for their skilled and accurate fabrication of the target and wedge absorbers used in this experiment. We appreciate the assistance given us by the operations staff of the Bevalac and thank members of the scanning/measuring team for their important contributions to the experiment.

This work was supported by the Director, Office of Energy Research, Division of Nuclear Physics of the Office of High Energy and Nuclear Physics of the U.S. Department of Energy under Contract DE-AC03-76SF00098.

## References

1. JASON Committee Report "Review of Physics Issues for Accelerator Inertial Fusion" 13-14 July 1982.

2.. W.H. Barkas and M.J. Berger, NAS-NRC Publication 1133, 103 (1964).

3. H.H. Heckman, B.L. Perkins, W.B. Simon, F.M. Smith and W.H. Barkas, Phys. Rev. 117, 544 (1960).

4. R.P. Henke and E.V. Benton, Phys. Rev. 139, A2017 (1965).

5. E.V. Benton and R.P. Henke, Nucl. Inst. and Methods, 67, 87 (1969).

6. For a late review of the literature on energy-loss processes of relativistic, highly-ionizing particles, see:
S.P. Ahlen, Rev. Mod. Phys. 52, 121 (1980), and references therein.

## Figure Captions

Fig. 1 a) Maximum beam energy for $^{197}Au$ at $p_{max} = 5.75\ Z_{accel}$ GeV/c.

b) Calculated effective charge at equilibrium, $Z^*_{equil}$, in CH.

c) Difference between curves b) and a); electron excess = $Z^*_{equil} - Z_{accel}$.

d) Schematic trajectory of the transition of Z* for Au beam nuclei, E = 152 MeV/amu, from $Z_{accel} = 19$ to $Z^*_{equil}$ when slowing down in CH.

Fig. 2 Schematic drawing of experimental configuration. TOF measurements are made over flight path $S_1S_2$. Trajectories of magnetically separated charge states of beam, $Z_i$, are indicated. Stop-counter $S_2$ is removed when the wedge-emulsion unit is in place.

Fig. 3 a) Cross section of CH wedge absorber with glass-backed 10 μm-thick emulsion in contact with back surface of wedge. Beam enters (from left) normal to plane of wedge-emulsion interface.

b) Photograph of emulsion detector exposed with CH-wedge absorber to 152 MeV/amu $Au^{+61}$ beam. Relative scale sizes of Figs. a) and b) are equal. The enhanced darkening of the emulsion is due to δ-rays produced in, and ejected from, the circular CH wedge. The lighter, central disk clearly defines the "hole" of the wedge.

c) The radial distribution of stopping Au ions observed in emulsion plate, b).

Fig. 4 Range-energy relation for Au ions in CH and Au absorbers. $Au^{+61}$ beam was incident at 152 MeV/amu. Data from the wedge-emulsion unit are indicated by ⊙; the $R_o - S_i$ data, where $R_o$ is the measured (wedge) range at beam energy and $S_i$ is the degrader foil thickness, are indicated by -!-. The dashed curves are least-squares fits. The continuous lines are predicted ranges from R-E code (Ref. 4).

Fig. 5 Energy-loss rates of Au in CH and Au absorbers versus energy. Symbols are the same as in Fig. 4.

Fig. 6 Effective charge Z* (Eq. 6) vs energy of Au ions incident at 152 MeV/amu, $Z_{accel} = 61$.

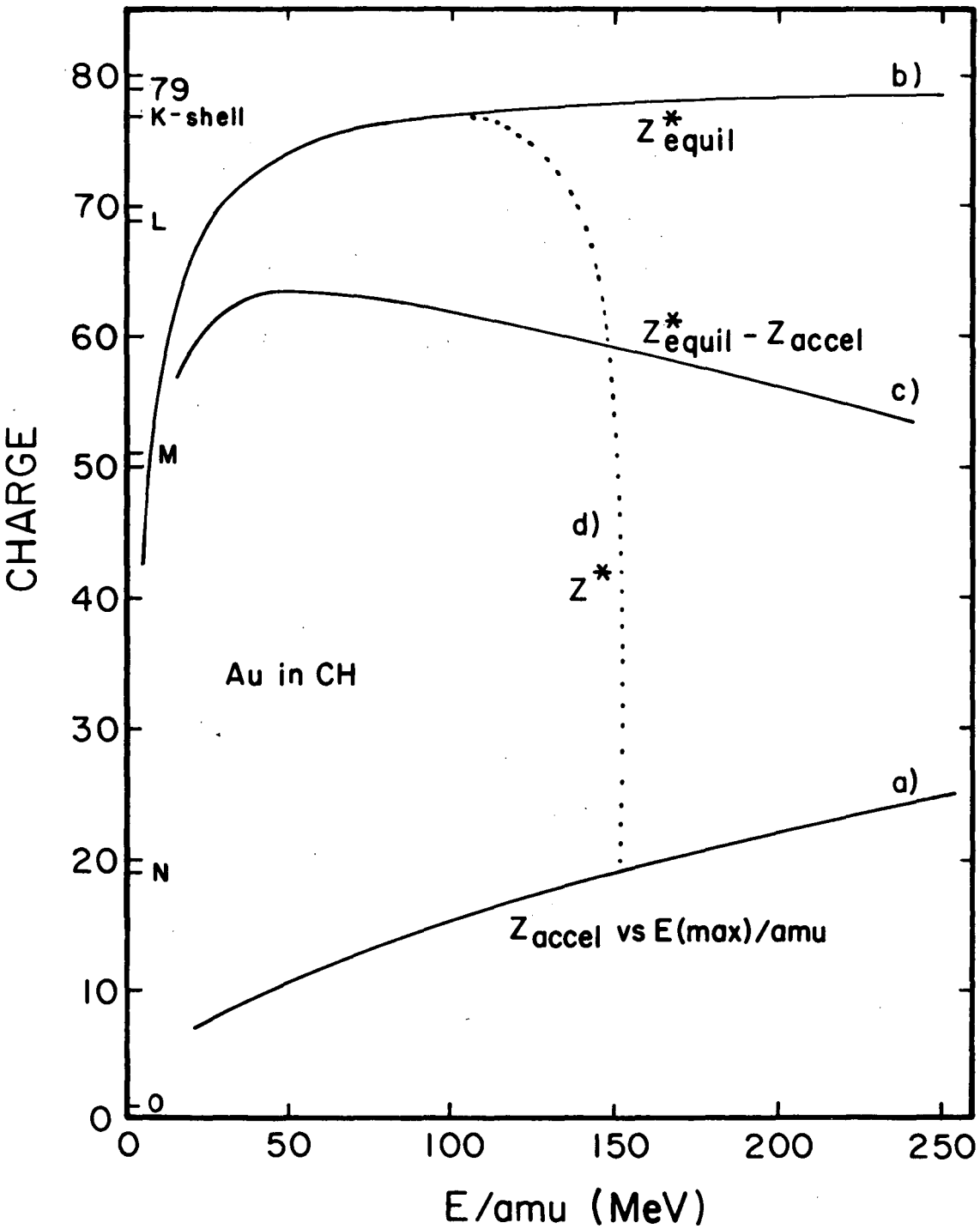


XBL 852-1078

Fig. 1

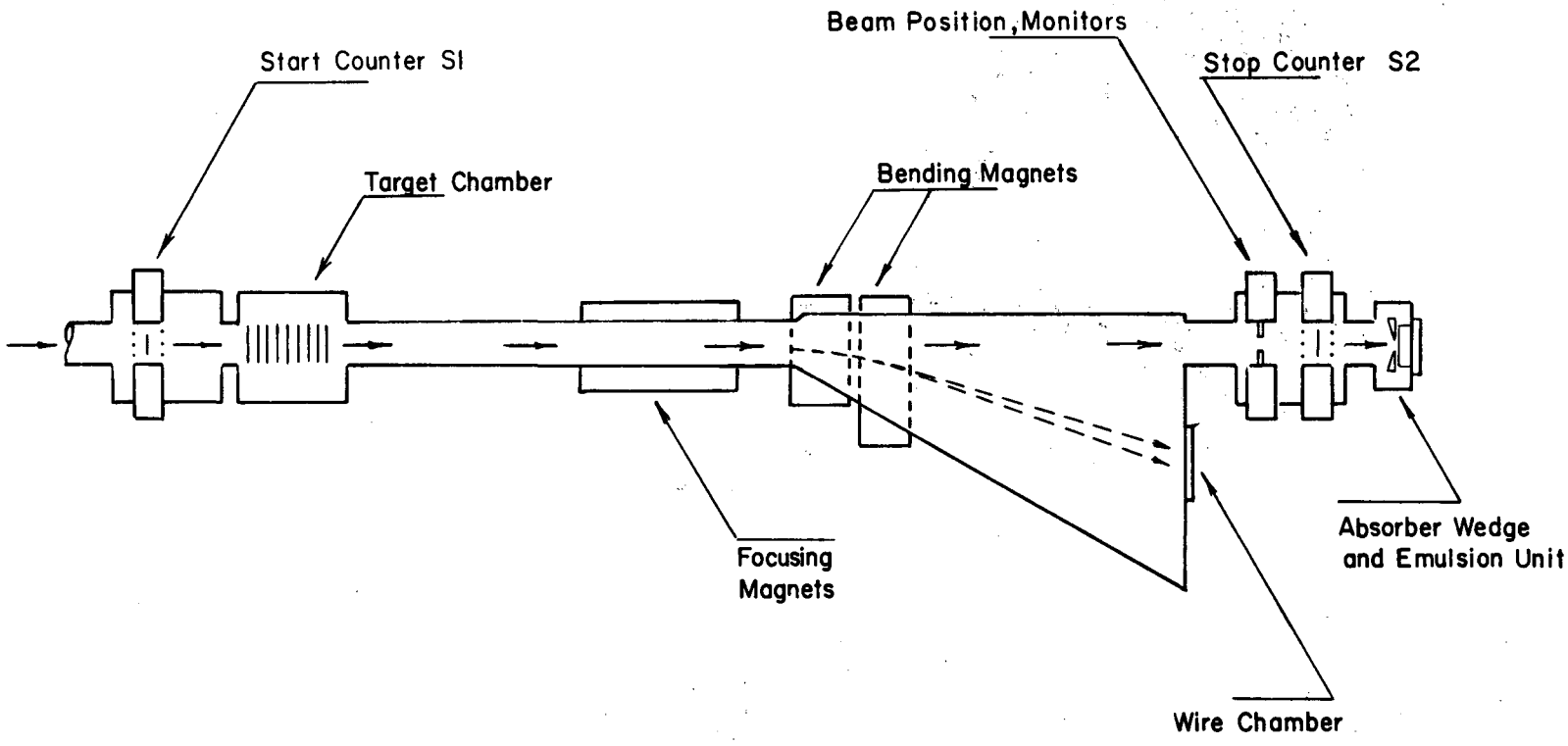
Beam Position, Monitors
Start Counter S1
Stop Counter S2
Target Chamber
Bending Magnets
Focusing Magnets
Absorber Wedge and Emulsion Unit
Wire Chamber
XBL 852-1079

Fig. 2

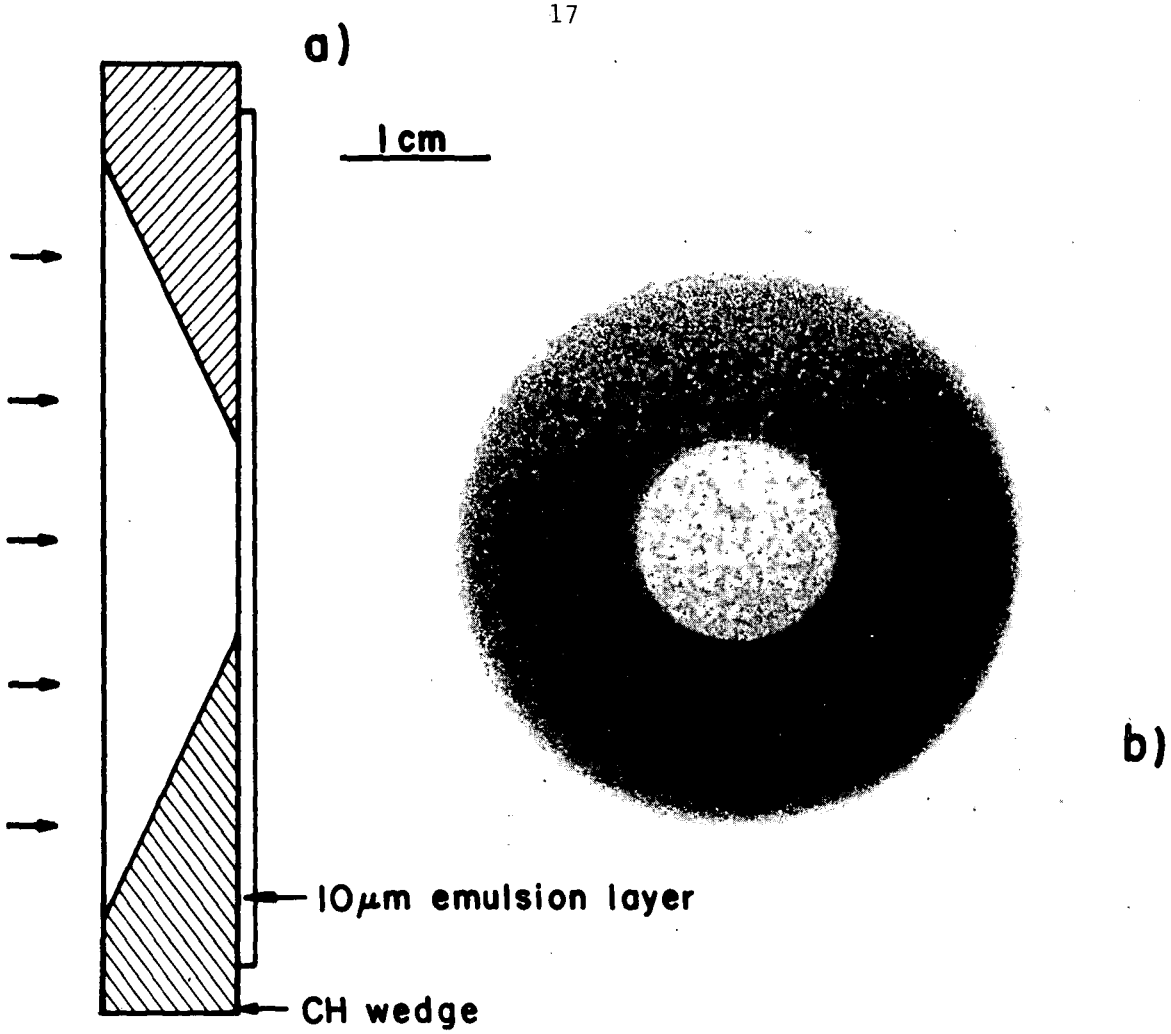


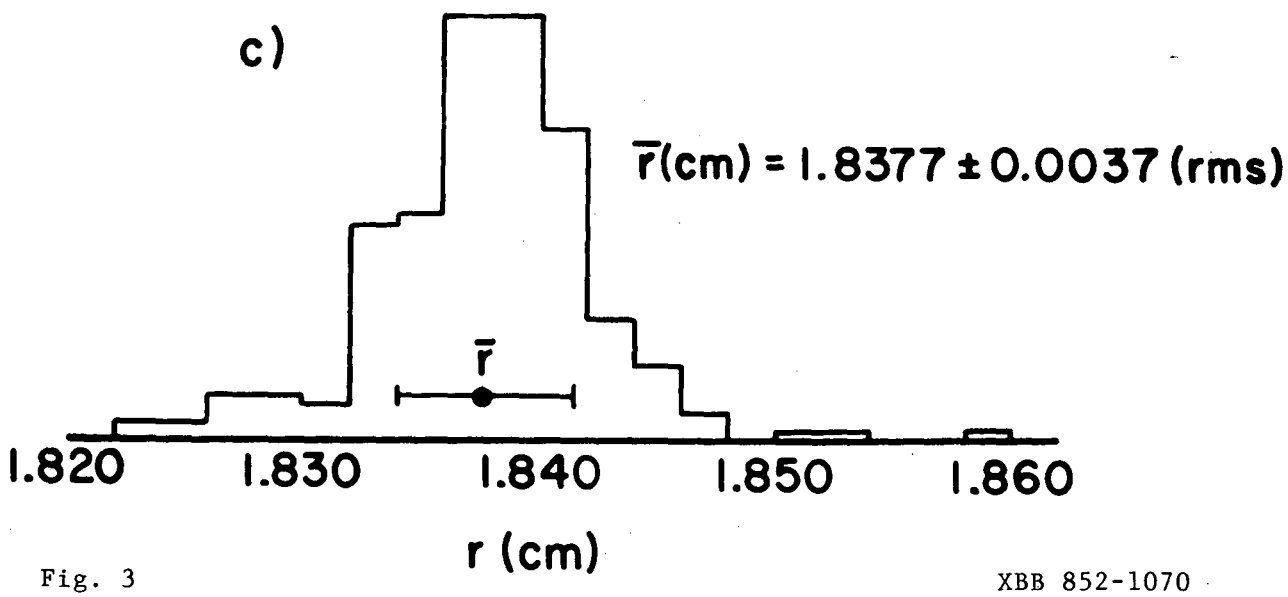


Fig. 3

XBB 852-1070

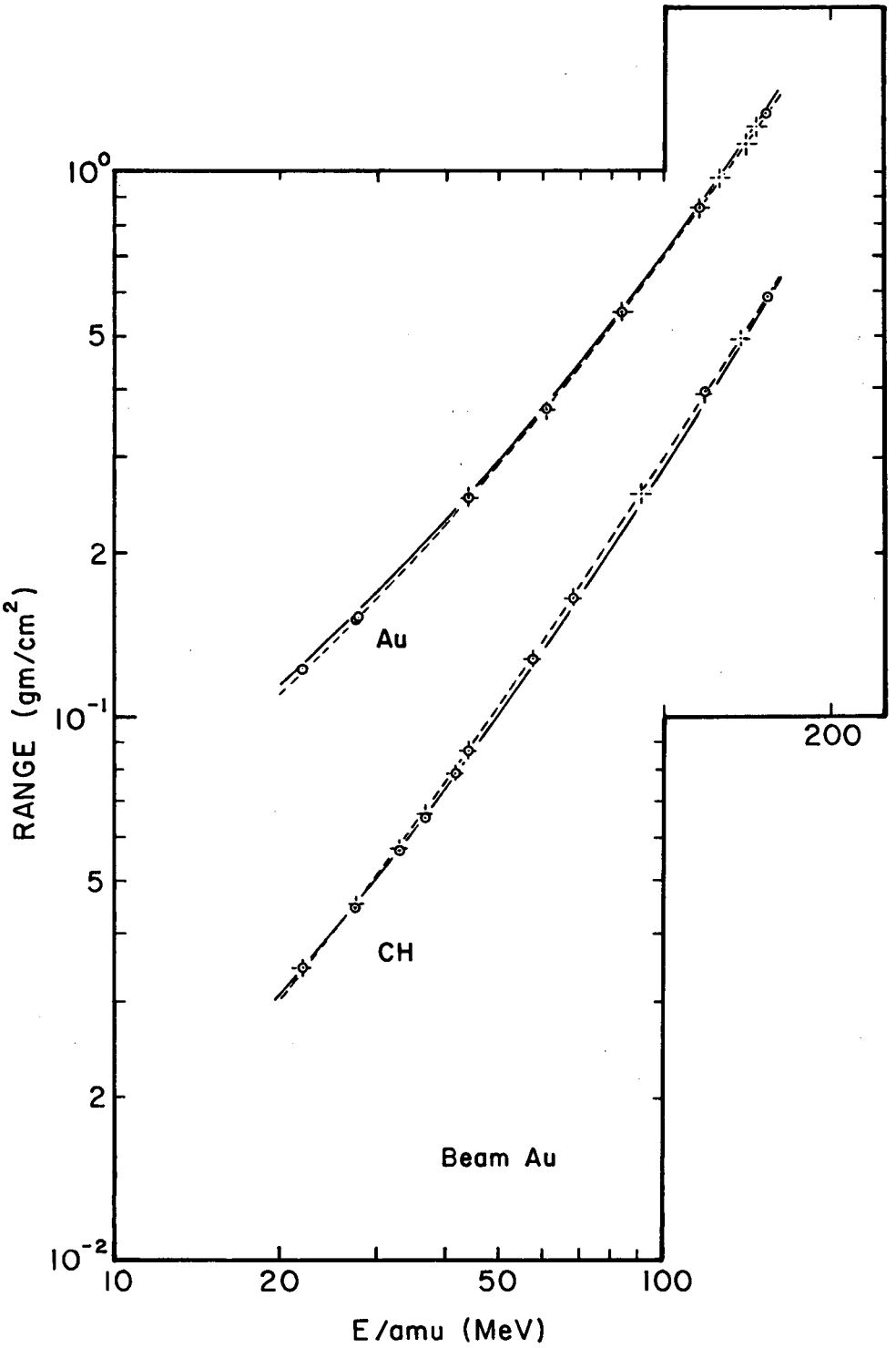


XBL 852-1080

Fig. 4

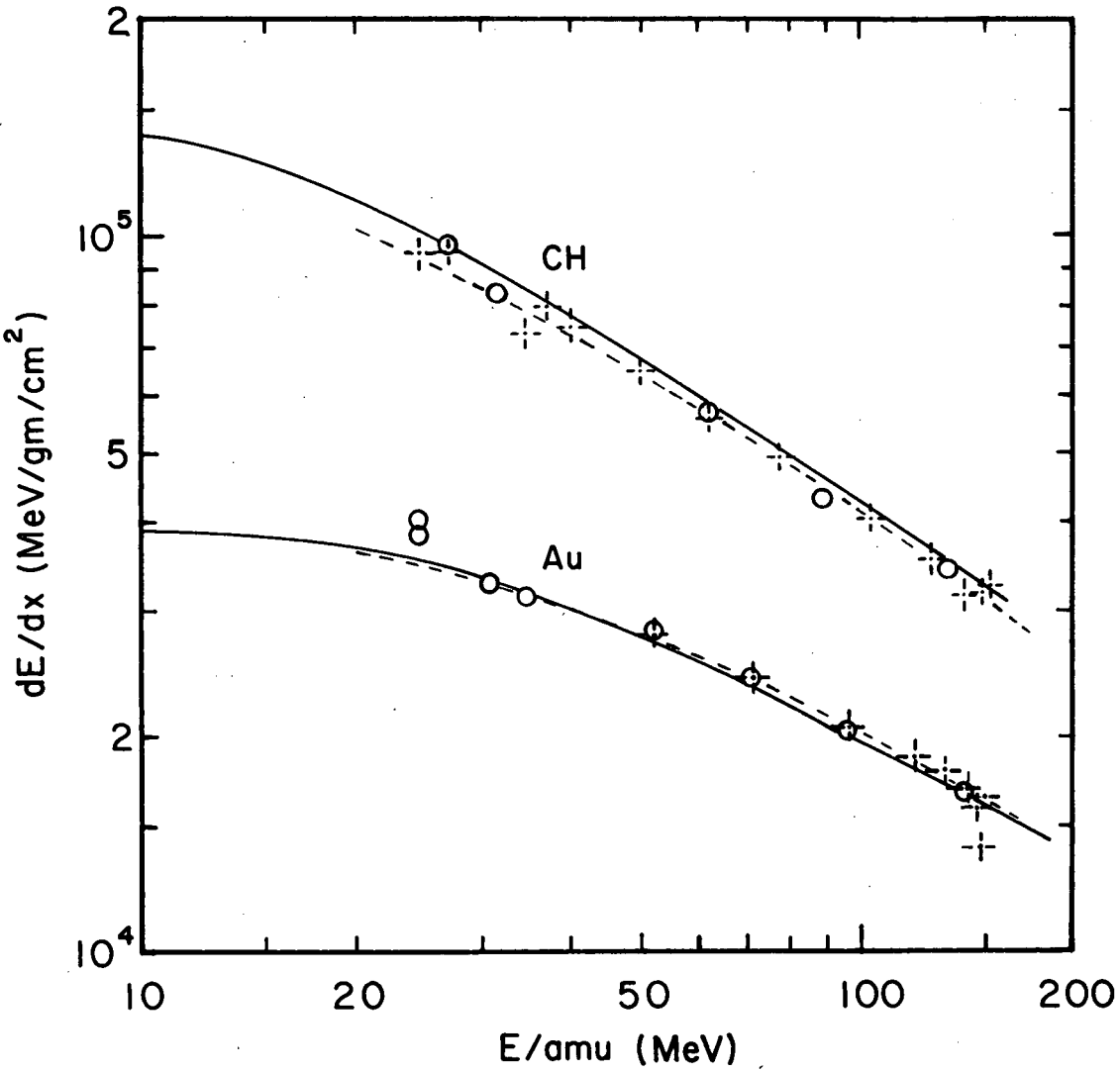


XBL 852-1081

Fig. 5

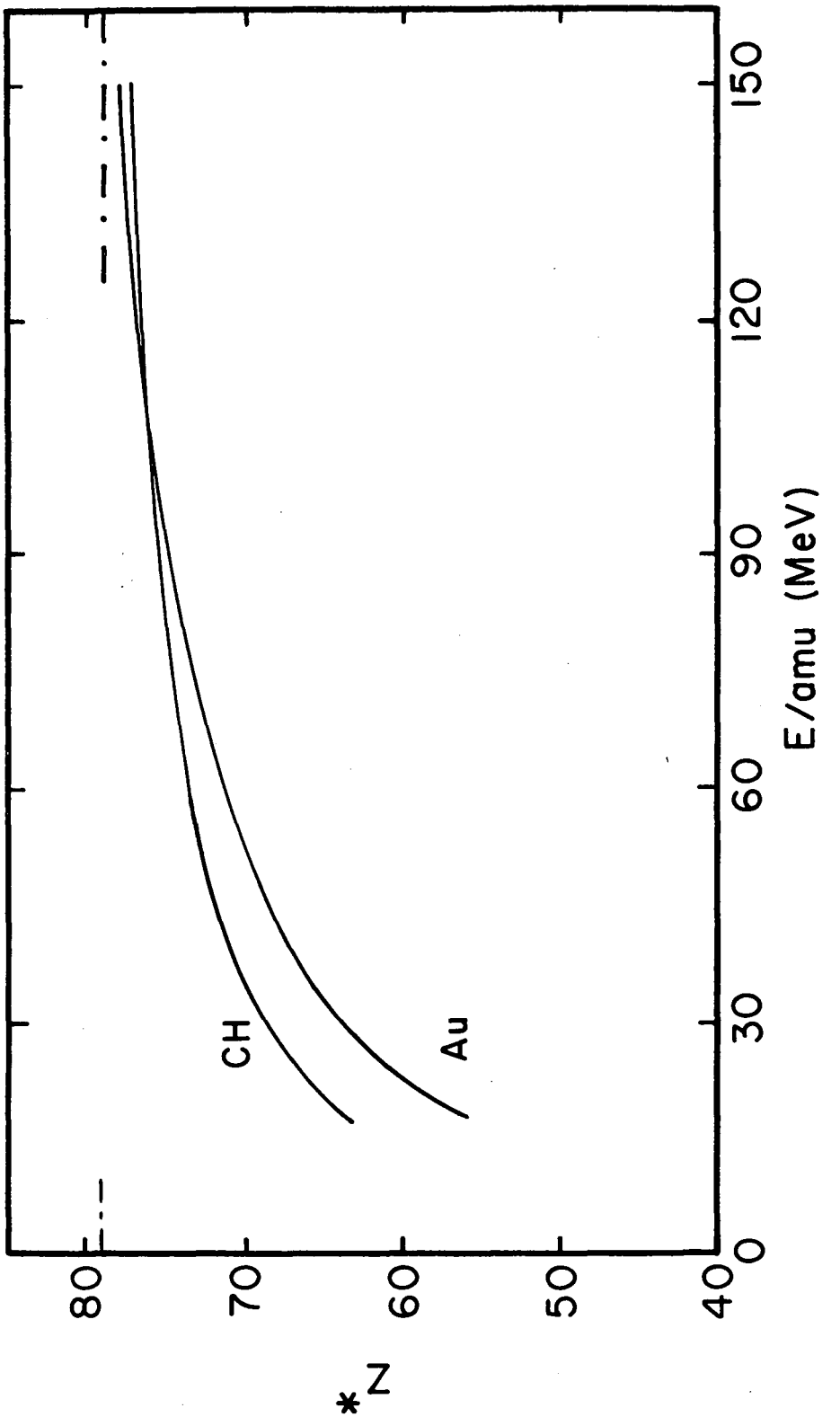


XBL 852-1077

Fig. 6

This report was done with support from the Department of Energy. Any conclusions or opinions expressed in this report represent solely those of the author(s) and not necessarily those of The Regents of the University of California, the Lawrence Berkeley Laboratory or the Department of Energy.

Reference to a company or product name does not imply approval or recommendation of the product by the University of California or the U.S. Department of Energy to the exclusion of others that may be suitable.

*TECHNICAL INFORMATION DEPARTMENT*
*LAWRENCE BERKELEY LABORATORY*
*UNIVERSITY OF CALIFORNIA*
*BERKELEY, CALIFORNIA 94720*